1-1-1986

Use of superposition to estimate power profiles in nuclear reactor fuel assemblies

Feyzi Inanc
Iowa State University

Use of superposition to estimate power profiles in nuclear reactor fuel assemblies

by

Feyzi Inanc

A Thesis Submitted to the
Graduate Faculty in Partial Fulfillment of the
Requirements for the Degree of
MASTER OF SCIENCE

Major: Nuclear Engineering

Iowa State University
Ames, Iowa

1986

TABLE OF CONTENTS

LIST OF TABLES

LIST OF FIGURES

INTRODUCTION

One of the important tasks to be performed by nuclear engineers in nuclear reactor analysis is determination of flux and power distributions in the reactor core. The common fine mesh finite difference techniques employed for this purpose in fuel management are not very attractive due to long computational time and large computer storage requirements for these methods. Techniques which have been developed since the early 1970s as alternatives to fine mesh techniques are nodal analyses of the reactor core. Although early versions of nodal models had been developed to calculate the core multiplication factor and average nodal powers, the later versions are capable of calculating local flux and power distributions as well [1,2]. Due to efforts being spent on the development of nodal techniques, they are expected to reach accuracy levels which will allow them to compete with fine mesh methods in the near future [2].

The nodal methods, which are basically neutron balance equations, can be considered as the combination of three successive procedures. The first procedure is to prepare homogenized neutronic parameters which will be used by the nodal equations. The success of the nodal techniques depends heavily on this first stage of computations. Although the most commonly applied technique for this purpose is to flux-weight heterogeneous neutronic

parameters, recently developed techniques based on "equivalence theory" are in the process of being adapted as the standard procedure for this purpose [3,4]. The second stage of the computations is the calculation of the core multiplication factor and the average nodal quantities such as average fluxes and average interface partial currents. Since the average quantities provided by the nodal calculations are not useful for a rigorous evaluation of the power distribution in the core, a third stage of calculations is required for determining the local flux and pin power distributions. The methods developed for this purpose can be grouped as normalization, flux-lupe and superposition methods [5].

The purpose of this thesis is to apply the superposition method to a PWR fuel assembly which simulates some PWR fuel assemblies located in a reactor core. In the nodal reactor analysis, the nodes are usually treated as small homogeneous reactors coupled to each other through partial currents. If the partial currents for a node as provided by the global calculations are used as boundary conditions for a single node with the same neutronic parameters, it should provide the same flux distribution as the one provided by the global calculation for that specific node. In this thesis, the power distributions generated from the simulated flux distributions in a PWR fuel for

various boundary conditions are superposed by the power peak factors and the local pin power distributions are obtained. Then these pin power distributions are compared to the reference pin power distributions to study the performance under varying conditions.

LITERATURE REVIEW

The first nodal methods ever developed were designed to calculate the global core eigenvalue and the average nodal powers [2]. The success of these methods in determining the mentioned quantities led to efforts for developing new nodal models capable of calculating nodal pin power distributions in an accurate manner. As a consequence of these efforts, the techniques called imbedded heterogeneous assembly calculations, superposition method and an analytical method have been developed in recent years [3,5,6,7,8]. The common point among these methods is that they are all employed after global reactor solution has been obtained by the nodal techniques. The other common points which can be observed are [2]:

1. they all use the outcomes of the nodal calculations for determining the pin power distributions,
2. they can be applied to each node or fuel assembly in a calculation independent of other nodes,
3. they usually employ transport techniques in one of the steps.

The imbedded assembly or flux-lupe technique was developed by Koebke and Wagner [6]. This technique employs an interpolation scheme which is used to approximate the spatially dependent interface partial currents from the

average interface partial currents. Once the spatially dependent partial currents are approximated, they are used in a fixed source transport calculation carried out for the heterogeneous fuel assembly. This technique is very succesful for very heterogeneous fuel assemblies, but it is not very efficient since it requires a fine mesh calculation. Koebke and Wagner report a maximum error of 1.7 % for an octant core which includes boron pins [6]. Nissen who also investigated the same method, reports an error of 0.90 % for a BWR fuel assembly calculation at the bottom of the core [5].

In the analytical approach reported, the heterogeneous flux is expressed as the product of a form function and flux peak factors [7,9]. This expression is substituted into the diffusion equation. These equations are solved for the form functions after some approximations are made. Then the form functions are used to evaluate the smooth flux profiles in triangles into which the fuel assemblies are partitioned. The flux values at the corner points which make up the conditions for the form functions are determined by an interpolation technique as developed by Koebke and Wagner [6].

The modulation or superposition method has also been developed by Koebke and Wagner [6]. This method includes an interpolation scheme for reconstructing the homogeneous flux

and power profiles. After the homogeneous power profiles are reconstructed, predetermined power peak factors are superpositioned on the homogeneous profiles to get the pin power distributions. This method is reported to be successful in the assemblies with few heteregoneities. For the assemblies with the control rods, the fuel assemblies are partitioned into more than one node to get better accuracy.

THE NODAL METHODS

The nodal methods are usually based upon establishing neutron balance equations in subregions of the reactor core. The neutron balance equations can be derived from either the neutron transport equation or from the neutron diffusion equation. The derivation of the equations does not involve any approximation and the nodal equations can provide exact integral node quantities if exact coupling relations can be found between the adjacent nodes. The determination of the coupling relations between the adjacent nodes is where the first approximations are introduced in the derivation of the equations. The derivation of the nodal equations in 2-D Cartesian geometry is outlined in the following section.

Since the nodal equations are neutron balance equations, we are concerned with the integral quantities within the nodes. If we use the diffusion equation to derive the nodal equations, we start by integrating the neutron diffusion equation over the x-y cross section of the node shown in Figure 1.

$$\iint_{A_{ij}} [-\nabla D_g(x,y)\nabla\phi_g(x,y)+\Sigma_{tg}(x,y)\phi_g(x,y)]dx\,dy =$$
$$\iint_{A_{ij}} [\chi_g \sum_{h=1}^{G} \nu\Sigma_{hf}(x,y)+ \sum_{h=1}^{G} \Sigma_{sgh}(x,y)]\phi_h(x,y)dx\,dy \qquad (3\text{-}1)$$

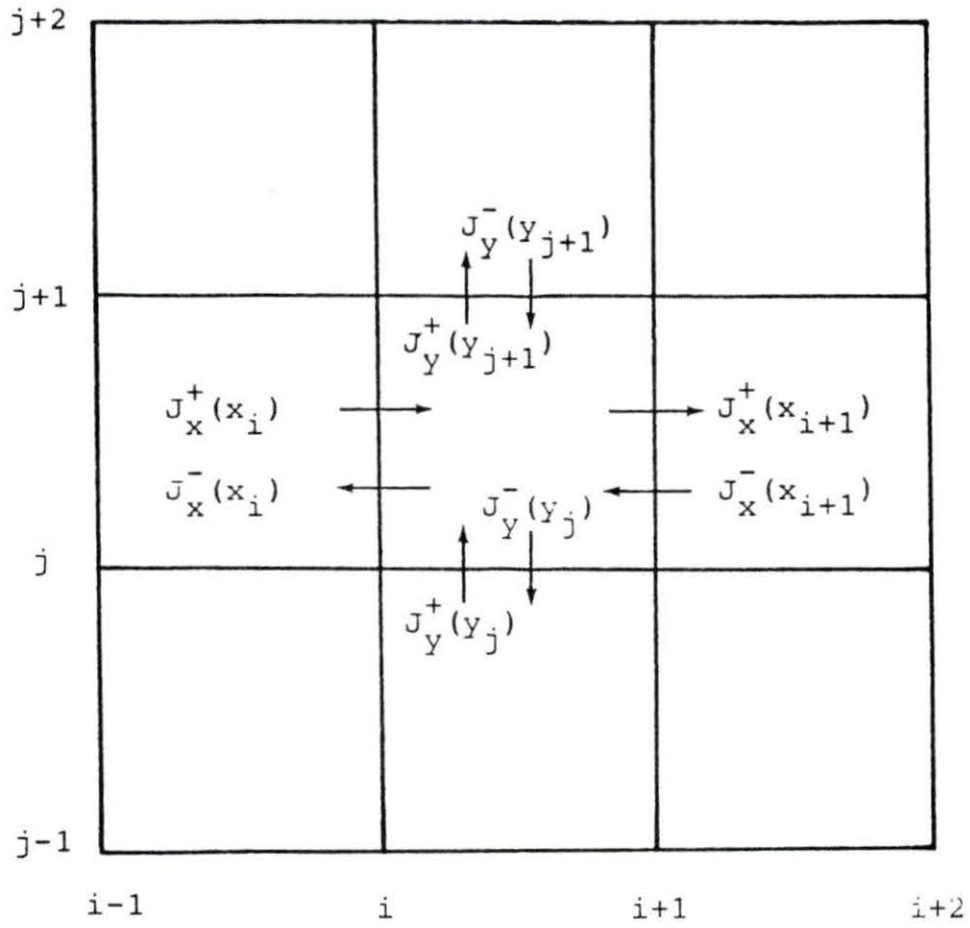

FIGURE 1. Adjacent nodes for development of the nodal equations

where:

ϕ_g neutron flux in group g

D_g diffusion coefficient for group g

Σ_{tg} total cross section for group g

χ_g fraction of fission neutrons born in group g

ν average number of neutrons released per fission

Σ_{fh} fission cross section for group h

Σ_{sgh} scattering cross section from group h to group g

The integration results in the following equation [10]

$$-[L_x+L_y]+A_{ij}\bar{\Sigma}_{tg}\bar{\phi}_g = A_{ij}\sum_{h=1}^{G}[\chi_g\nu\bar{\Sigma}_{fh}+\bar{\Sigma}_{sgh}]\bar{\phi}_h \qquad (3\text{-}2)$$

where:

$J_x(x)$ is average neutron current in x direction

$J_y(y)$ is average neutron current in y direction

$$L_x = J_x(x_{i+1})-J_x(x_i)$$

$$L_y = J_y(y_{j+1})-J_y(y_j)$$

$$\bar{\Sigma}_\alpha = \frac{1}{\phi_{tot}}\iint_{A_{ij}} \Sigma_\alpha(x,y)\phi(x,y)dx\,dy$$

$$\bar{\phi}_{ij} = \frac{1}{A_{ij}}\iint_{A_{ij}} \phi(x,y)dx\,dy$$

$$\phi_{tot} = \iint_{A_{ij}} \phi(x,y)dx\,dy$$

If the currents at the interfaces are expressed in terms of partial interface currents, we can get the neutron balance equations.

$$\frac{1}{h}[J_x^+(x_{i+1})-J_x^-(x_{i+1})+J_x^+(x_i)-J_x^-(x_i)]$$

$$+\frac{1}{h}[J_y^+(y_{j+1})-J_y^-(y_{j+1})+J_y^+(y_j)-J_y^-(y_j)]$$

$$+\bar{\Sigma}_{tg}\bar{\phi}_g - \sum_{h=1}^{G}[\chi_g\nu\bar{\Sigma}_{fh}+\bar{\Sigma}_{sgh}]\bar{\phi}_h = 0 \qquad (3\text{-}3)$$

where:

$J_x^+(x)$ average partial current in positive x direction

$J_x^-(x)$ average partial current in negative x direction

$J_y^+(y)$ average partial current in positive y direction

$J_y^-(y)$ average partial current in negative y direction

As can be seen from equation (3-3), the average flux for node ij, shown in Figure 1, can be calculated if partial currents at the node interfaces are known. Two common methods for establishing coupling relations between the adjacent nodes are collision probability methods and polynomial expansion methods. They both express the outgoing partial currents in terms of incoming currents and average node fluxes.

Collision Probability Method

This method employs escape and transfer probability methods for expressing outgoing currents in terms of incoming partial currents and node average fluxes [1,10,11] in the following manner.

$$J_x^+(x_{i+1}) = A_{ij} \sum_{h=1}^{G} (\chi_g \nu\bar{\Sigma}_{fh} + \bar{\Sigma}_{sgh}) P_E(x_{i+1}) \bar{\phi}_h +$$

$$(J_x^-(x_{i+1}) + J_x^+(x_i) + J_y^-(y_{j+1}) + J_y^+(y_j)) P_T(x_{i+1}) \qquad (3\text{-}4a)$$

$$J_x^-(x_i) = A_{ij} \sum_{h=1}^{G} (\chi_g \nu\bar{\Sigma}_{fh} + \bar{\Sigma}_{sgh}) P_E(x_i) \bar{\phi}_h^+$$

$$(J_x^-(x_{i+1}) + J_x^+(x_i) + J_y^-(y_{j+1}) + J_y^+(y_j)) P_T(x_i) \qquad (3\text{-}4b)$$

$$J_y^+(x_{j+1}) = A_{ij} \sum_{h=1}^{G} (\chi_g \nu\bar{\Sigma}_{fh} + \bar{\Sigma}_{sgh}) P_E(y_{j+1}) \bar{\phi}_h^+$$

$$(J_x^-(x_{i+1}) + J_x^+(x_i) + J_y^-(y_{j+1}) + J_y^+(y_j)) P_T(y_{j+1}) \qquad (3\text{-}4c)$$

$$J_y^-(x_j) = A_{ij} \sum_{h=1}^{G} (\chi_g \nu\bar{\Sigma}_{fh} + \bar{\Sigma}_{sgh}) P_E(y_j) \bar{\phi}_h^+$$

$$(J_x^-(x_{i+1}) + J_x^+(x_i) + J_y^-(y_{j+1}) + J_y^+(y_j)) P_T(y_j) \qquad (3\text{-}4d)$$

where:

$P_E(s)$ = Probability for neutrons born in node ij to escape through surface s.

$P_T(s)$ = Probability for neutrons entering node ij from nodes (i,j+1),(i+1,j),(i,j-1),(i-1,j) to escape through surface s.

Determination of escape probabilities depend on the neutron sources very strongly. This requires some assumptions to be made for the source shapes. One assumption is to use flat source distributions. Since this is a very crude approximation, it usually leads to insufficient accuracy [1]. An alternative for the flat source is to use quadratic polynomials for the neutron flux shapes as below:

$$\psi(u_x) = \bar{\phi}+\frac{1}{2}[\psi_x(x_{i+1})-\psi_x(x_i)].(2u_x-1)+$$

$$\frac{1}{2}[2\bar{\phi}-\psi_x(x_{i+1})-\psi_x(x_i)].(6u_x-6u_x^2-1) \qquad (3\text{-}5a)$$

$$\psi(u_y) = \bar{\phi}+\frac{1}{2}[\psi_y(y_{j+1})-\psi_y(y_j)].(2u_y-1)+$$

$$\frac{1}{2}[2\bar{\phi}-\psi_y(y_{j+1})-\psi_y(y_j)].(6u_y-6u_y^2-1) \qquad (3\text{-}5b)$$

where:

$$\psi(u_y) = \int_0^{a_x} \phi(x,y)dx$$

$$\psi(u_x) = \int_0^{a_y} \phi(x,y)dy$$

$$u_x = \frac{x}{a_x}, \qquad u_y = \frac{y}{a_y} \qquad (0\leq u\leq 1)$$

These quadratic equations are used to calculate the escape probabilities for each iteration.

Polynomial Expansion Method

The starting point for the polynomial expansion method is to integrate the diffusion equation over one dimension and to reduce it to one dimensional equation in the following way [12]:

$$-D_g \frac{d}{dx}\left(\frac{d}{dx}\psi_g(x)\right)+L_y(x)+\bar{\Sigma}_{tg}\psi_g(x) = \sum_{h=1}^{G} (\chi_g \nu\bar{\Sigma}_{fh}+\bar{\Sigma}_{sgh})\psi_h(x) \qquad (3\text{-}6a)$$

$$-D_g \frac{d}{dy}\left(\frac{d}{dy}\psi_g(y)\right)+L_x(y)+\bar{\Sigma}_{tg}\psi_g(y) = \sum_{h=1}^{G} (\chi_g \nu\bar{\Sigma}_{fh}+\bar{\Sigma}_{sgh})\psi_h(y) \qquad (4\text{-}6b)$$

where:

$$\psi(x) = \int \phi(x,y)dy$$

$$\psi(y) = \int \phi(x,y)dx$$

$$L_y(x) = J_y(x,y_{j+1})-J_y(x,y_j)$$

$$L_x(y) = J_x(x_{i+1},y)-J_x(x_i,y)$$

The next step is to expand the one dimensional flux as a high order polynomial as given by [12]:

$$\psi(x) = \int_0^{a_y} \sum_{i,j=0}^{i+j\leq 2+n} c_{ij}h_i\left(\frac{x}{a_x}\right)h_j\left(\frac{y}{a_y}\right)dy \qquad (3\text{-}7a)$$

$$\psi(y) = \int_0^{a_x} \sum_{i,j=0}^{i+j\leq 2+n} c_{ij}h_i\left(\frac{x}{a_x}\right)h_j\left(\frac{y}{a_y}\right)dx \qquad (3\text{-}7b)$$

where:

$$h_0 = 1$$

$$h_1 = 2u-1$$

$$h_2 = 6u(u-1)-1$$

$$h_3 = 6u(1-u)(2u-1)$$

$$h_4 = 6u(1-u)(5u^2-5u+1)$$

$$h_5 = 6u(1-u)(2u-1)(6u^2-6u+1)$$

The first five coefficients of the polynomial are obtained by using the following conditions.

$$-D\frac{d}{dx}(\frac{d\psi}{dx}) = J_x^+(x_{i+1})-J_x^-(x_{i+1}) \quad \text{at } x=x_{i+1} \tag{3-8a}$$

$$\psi(x_{i+1}) = 2[J_x^+(x_{i+1})+J_x^-(x_{i+1})] \tag{3-8b}$$

$$-D\frac{d}{dx}(\frac{d\psi}{dx}) = J_x^-(x_i)-J_x^+(x_i) \quad \text{at } x=x_i \tag{3-8c}$$

$$\psi(x_i) = 2[J_x^+(x_i)+J_x^-(x_i)] \tag{3-8d}$$

$$\bar{\phi} = \frac{1}{a_x}\int_0^{a_x} \psi(x)dx \tag{3-8e}$$

The rest of the coefficients are calculated by using the weighted residual method. An analogous scheme is applied to find $\psi(y)$.

If the transverse leakage terms in equations (3-6a) and (3-6b) can be approximated, outgoing partial currents can be obtained from the equations since $\psi(x)$ and $\psi(y)$ are known in terms of the polynomials. The transverse leakages can be approximated by a parabolic equation [11,13].

$$L_x(y) = C_0+C_1h_1(\frac{y}{a_y})+C_2h_2(\frac{y}{a_y}) \tag{3-9a}$$

$$L_y(x) = B_0 + B_1 h_1\left(\frac{x}{a_x}\right) + B_2 h_2\left(\frac{x}{a_x}\right) \qquad (3\text{-}9b)$$

Coefficients for the equations (3-9a) and (3-9b) are found by using the following conditions:

$$\bar{L}_y = \frac{1}{a_x}\int_0^{a_x} L_y(x)dx \qquad (3\text{-}10a)$$

$$L^{i-1,j}_y(x_i) = L^{i,j}_y(x_i) \qquad (3\text{-}10b)$$

$$L^{i+1,j}_y(x_{i+1}) = L^{i,j}_y(x_{i+1}) \qquad (3\text{-}10c)$$

$$\bar{L}_x = \frac{1}{a_y}\int_0^{a_y} L_x(y)dy \qquad (3\text{-}10d)$$

$$L^{i,j+1}_x(y_{j+1}) = L^{i,j}_x(y_{j+1}) \qquad (3\text{-}10e)$$

$$L^{i,j-1}_x(y_j) = L^{i,j}_x(y_j) \qquad (3\text{-}10f)$$

If the equations (3-9a) and (3-9b) are substituted into equations (3-6a) and (3-6b), outgoing currents in these two equations can be written in terms of incoming partial currents and node average fluxes. Then these outgoing partial currents are used to eliminate the outgoing partial currents which appear in equation (3-3). After that an iterative technique is employed to solve the nodal equations for the average fluxes. The incoming partial currents from the previous iteration are used to calculate the node average flux from equation (3-3). This updated average flux

and the incoming partial currents are used to update the outgoing partial current which is to be used by the adjacent nodes as incoming partial current.

HOMOGENIZATION OF NEUTRONIC PARAMETERS

As was discussed in the third chapter, the nodal equations are derived for homogenized regions. Since fuel assemblies are not homogenous, the neutronic parameters should be homogenized in some way. The success of ıe nodal methods is heavily dependent upon finding properly homogenized neutronic parameters.

The homogenized neutronic parameters which will be used in the nodal equations must have the following characteristics for an exact representation of a heterogenous core region [14]:

1. they should be constant over a given volume V_i,
2. they should provide the same integral reaction rates as were provided by the heterogenous parameters,
3. they should provide the same eigenvalue as was provided by the heterogenous parameters.

These conditions can be met if the following expressions can be satisfied.

$$\int_{V_i} \frac{d}{du}[J_u(r)]dV = -[\bar{D}_u]_i \int_{V_i} \frac{d}{du}\left(\frac{d}{du}[\bar{\phi}(r)]\right)dV \qquad (4\text{-}1)$$

$(u=x,y,z)$

$$\int_{V_i} [A(r)][\phi(r)]dV = [\bar{A}]_i \int_{V_i} [\phi(r)]dV \qquad (4\text{-}2)$$

$$\int_{V_i} [M(r)][\phi(r)]dV = [\bar{M}]_i \int_{V_i} [\bar{\phi}(r)]dV \qquad (4\text{-}3)$$

where:

$$[\phi(r)] = \text{Col } \{\phi_1(r), \phi_2(r), \ldots\ldots, \phi_G(r)\}$$

$$[J_u(r)] = \text{Col } \{J_{1u}(r), J_{2u}(r), \ldots\ldots, J_{Gu}(r)\}$$

$$A_{gh}(r) = \Sigma_{tg}(r)\,\delta_{gh} - \Sigma_{sgh}(r)$$

$$[A(r)] = \{A_{gh}(r)\}, \text{ a GxG matrix}$$

$$[\nu^i \Sigma_f^i] = \text{Col } \{\nu_1^i \Sigma_{f1}^i(r), \ldots\ldots, \nu_G^i \Sigma_{fG}^i(r)\}$$

$$[\chi^i] = \text{Col } \{\chi_1^i, \chi_2^i, \ldots\ldots, \chi_G^i\}$$

$$[M(r)] = \sum_i [\chi^i][\nu^i \Sigma_f^i]^T$$

Although some new techniques have been proposed for homogenizing the neutronic parameters [3,4], the flux-weighting method still has a common application for this purpose. In contrast with its simplicity, it has serious theoretical weaknesses. Due to several approximations which will be outlined below, it has a limited range of application. This causes large errors in BWR power predictions [3]. In this technique, the homogenized neutronic parameters can be expressed as below:

$$[\bar{M}]_i = \frac{1}{[\phi]_{tot}} \int_{V_i} [M(r)][\phi(r)]dV \qquad (4\text{-}4)$$

$$[\bar{A}]_i = \frac{1}{[\phi]_{tot}} \int_{V_i} [A(r)][\phi(r)]dV \qquad (4\text{-}5)$$

$$[\bar{D}_u]_i = \{\int_{V_i} [\frac{d}{du}(\frac{d}{du}\phi(r))]dV\}^{-1} \int_{V_i} \frac{d}{du}[J_u(r)]dV \qquad (4\text{-}6)$$

where:

$$[\phi]_{tot} = \int_{V_i} [\bar{\phi}(r)]dV$$

If the equations (4-4),(4-5) and (4-6) are studied, it is easily seen that calculation of the homogenized parameters requires heterogenous fluxes to be known beforehand. Another problem associated with that is, even though heterogenous fluxes are assumed to be known, the calculation of homogenized parameters for each node is a time consuming procedure. The general approach to avoid these difficulties is to solve an eigenvalue problem for a fuel assembly with reflective albedo conditions and to use that flux distribution for all the fuel assemblies which have the same material properties. Although this is a good approximation for the fuel assemblies near the center of the reactor core, it is not a valid approximation near the periphery of the core where large flux gradients may occur.

Another problem lies with equations (4-2) and (4-3). These equations are in fact in vector forms as shown by equation (4-7).

$$\bar{A}_{1i}\int_{V_i}\bar{\phi}_1(r)dV + \bar{A}_{2i}\int_{V_i}\bar{\phi}_2(r)dV + .. + \bar{A}_{Gi}\int_{V_i}\bar{\phi}_G(r)dV =$$

$$\int_{V_i} A_1(r)\phi_1(r)dV + \int_{V_i} A_2(r)\phi_2(r)dV + ..$$

$$+ \int_{V_i} A_G(r)\phi_G(r)dV \qquad (4\text{-}7)$$

Even though all the heterogenous fluxes are assumed to be known, equation (4-7) consists of G unknown homogenized parameters. This difficulty can be overcome if the integral reaction rates of the homogenized and the heterogenous regions are taken to be equal in each energy group separately as shown in equation (4-8).

$$\bar{A}_{gi}\int_{V_i}\bar{\phi}_g(r)dV = \int_{V_i} A_{gi}(r)\phi_{gi}(r)dV \quad g=1,..,G \qquad (4\text{-}8)$$

The major approximation made in this homogenization technique is in the determination of the homogenized flux shapes which are denominators of the equations (4-4),(4-5) and (4-6). Since the determination of the homogenized fluxes is the target of the nodal analysis, there is no way of knowing these fluxes at the starting point. The routine way of approximating these fluxes is to use predetermined heterogenous fluxes to replace the homogenized fluxes. With that approximation, equations (4-4), (4-5) and (4-6) become:

$$\bar{D}_{ugi} = \{\int_{V_i}\frac{d}{du}(\frac{d}{du}\phi(r))dV\}^{-1}\int_{V_i}\frac{d}{du}J_{ug}(r)dV \qquad (4\text{-}9)$$

$(u=x,y,z), \quad g=1,..,G$

$$\bar{A}_{gi} = \frac{1}{\phi_{tot}} \int_{V_i} A_g(r)\phi_g(r)dV \qquad (4\text{-}10)$$

$$\bar{M}_{gi} = \frac{1}{\phi_{tot}} \int_{V_i} M_g(r)\phi_g(r)dV \qquad (4\text{-}11)$$

where:

$$\phi_{tot} = \int_{V_i} \phi_g(r)dV$$

The last difficulty with the method lies with the determination of the homogenized diffusion coefficient. The diffusion coefficient is a directional quantity and three separate homogenized quantities are required for the exact representation. These three coefficients can be reduced to one coefficient if the node is assumed to be a perfectly symmetric region either materialwise or flux-gradient-wise. If the requirement for the conservation of the integrated neutron is replaced by the conservation of the integrated transport reaction rate, the equation for determining a homogenized diffusion coefficient can be written in the form of the following equation.

$$\frac{1}{\bar{D}_{gi}} = \frac{1}{\phi_{tot}} \int_{V_i} \frac{1}{D_g(r)}\phi_g(r)dV \qquad (4\text{-}12)$$

As it can be seen from the discussion given above, the flux-weighing method is not an exact formulation. It contains several approximations and assumptions. In spite of this fact, this method has been used extensively for

homogenizing the neutronic parameters especially in cases where there are not large flux gradients over the region to be homogenized.

THE METHOD OF SUPERPOSITION

The method of superposition, as applied in this thesis, is simply to superpose the local power distribution within a node upon a power distribution calculated for a fuel assembly with homogenized neutronic parameters. The superposition method divides the determination of the detailed power distribution into two stages. In the first stage, the effects of the material heterogeneities is removed from the calculations by homogenizing the neutronic parameters of the fuel assembly. As a result of this homogenization, the power distributions, determined from the nodal model for example, would have the gradients imposed by the boundary conditions and the general power levels preserved. The introduction of the effects of the heterogeneities to the power distributions is done by superposing a more detailed, local power distribution upon the smooth power distributions determined in the first stage.

As can be seen from Figure 2, a typical PWR fuel assembly, even if the individual "pin cells" are homogenized, still has a heterogeneous structure. The existence of heterogeneities in the fuel assembly would require a fine mesh technique to be used for rigorous determination of the pin power distribution.

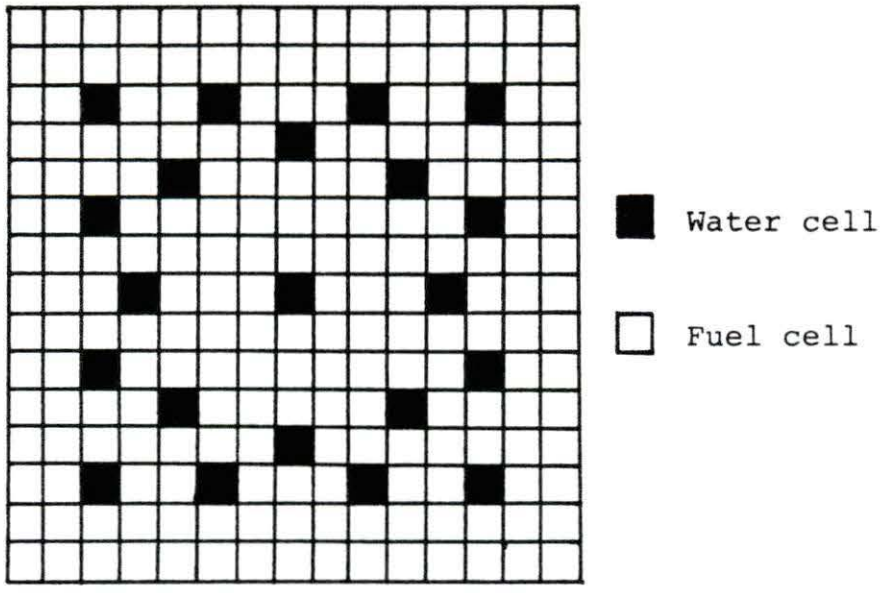

The heteregenous fuel assembly

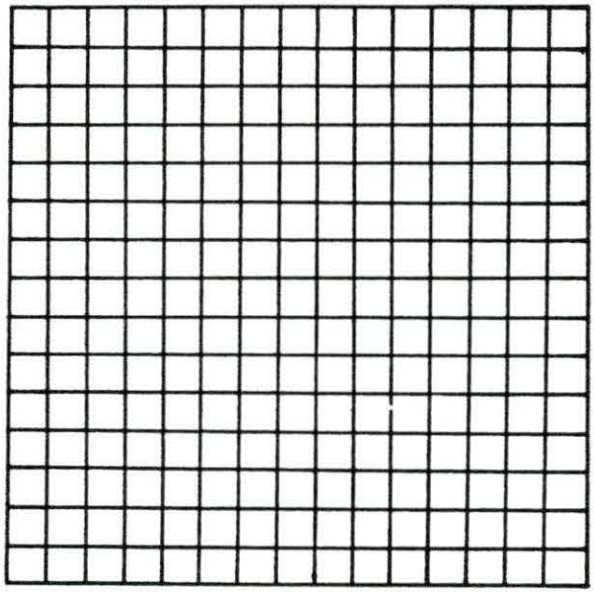

The homogenized fuel assembly

FIGURE 2. The heterogeneous and the homogenized fuel assemblies

The detailed effects of the material characteristics upon the power distribution are only weakly dependent on the boundary conditions imposed on the fuel assembly. As a result of this weak dependence, the effects of the material characteristics on the power distribution can be determined with an eigenvalue calculation by using a zero current boundary condition. This boundary condition removes all gradients which can be imposed by the adjacent nodes, and the power distribution resulting from this calculation would reflect only the effects of the heterogeneous character of the fuel assembly. This power distribution determined by using zero current boundary condition can be normalized by dividing the power distribution by the average assembly power. This normalization would result in the "power peak factors". Then, we multiply the smooth power distributions simulating the nodal solutions for various conditions by the power peak factors to determine the local pin power distributions. The scheme for the superposition method is outlined in Figure 3.

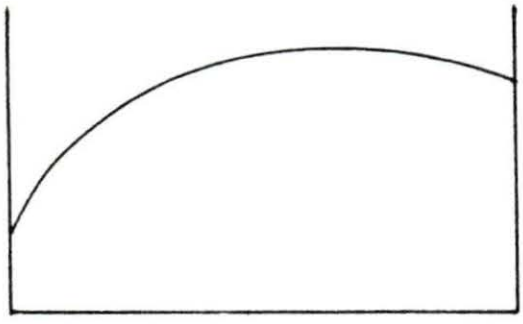

a) Smooth power distribution provided by nodal solution

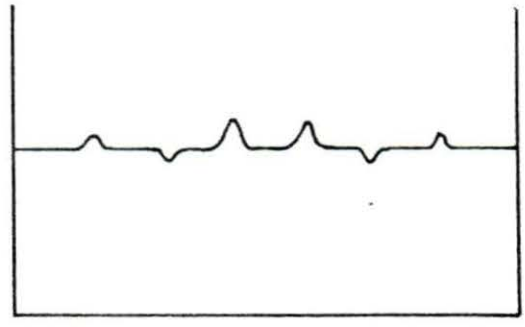

b) Power peak factors provided by a fine mesh calculation with perfectly reflected boundary conditions

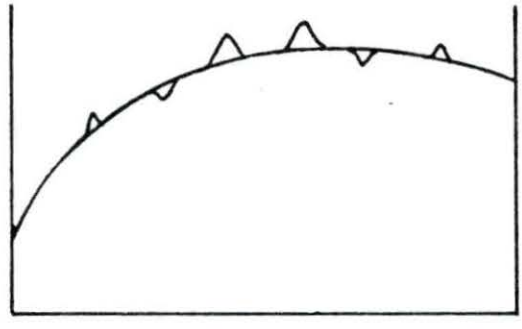

c) Superposition of power peak factors (b) upon the smooth power distribution (a)

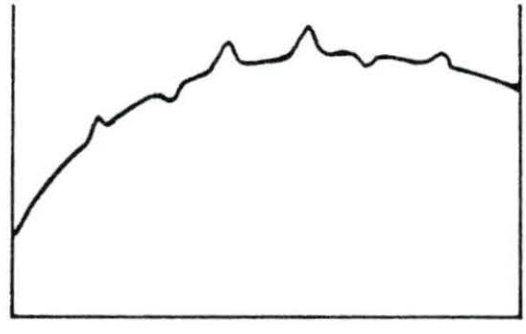

d) Pin power distribution simulating fine mesh calculations with identical boundary conditions for smooth power distribution case

FIGURE 3. The schematic representation of the superposition method in one dimension

APPLICATION OF THE METHOD

The application of the superposition method in this thesis is carried out in two stages. The first stage covers the preparation of homogenized neutronic parameters and power peak factors. The second stage involves determination of general features of power distribution for the homogenized fuel assembly and regeneration of the local pin power distribution by superposition. In this thesis, performance of the method is also evaluated by comparing the results with a reference solution.

Preparation of the Input Data

The homogenization of the neutronic parameters is done by using the flux-weighting method discussed in the fourth chapter. An eigenvalue calculation is carried out with the zero current boundary condition, and the resulting flux distribution is used to homogenize the neutronic parameters by using equations (4-10),(4-11) and (4-12). The neutronic parameters obtained from this homogenization process are assumed to represent the heterogeneous fuel assembly.

As explained in the fifth chapter on the superposition method, power peak factors are also determined from eigenvalue calculation with zero current boundary conditions. Since both the homogenization of the neutronic parameters and the determination of the power peak factors

require an eigenvalue calculation with zero current boundary conditions, the same calculation serves for both purposes. The eigenvalue calculation is carried out with the finite difference code DTDMG [15] by using space dependent neutronic parameters in the fuel assembly. The scheme used for these local calculations is shown in Figure 4.

Construction of Pin Power Distribution

Although the power peak factors are conventionally obtained from zero current calculations, the superposition method could be applied more accurately to the results of a global calculation. In our application, the global calculation provides boundary conditions to simulate the distributon of flux in a fuel assembly in a reactor core. The coarse mesh methods treat the core subregions as small homogeneous reactors coupled to the other regions through boundary conditions. If equation (3-3), which gives the nodal neutron balance expression, is studied, it can be seen that the flux within a node can be determined if the partial interface currents are known. In this work, we retain the power peak factors computed for the heterogeneous assembly, but apply them to fluxes within the homogenized node determined from these interface currents.

If the interface partial currents for a fuel assembly are taken from the converged global solution and used as the

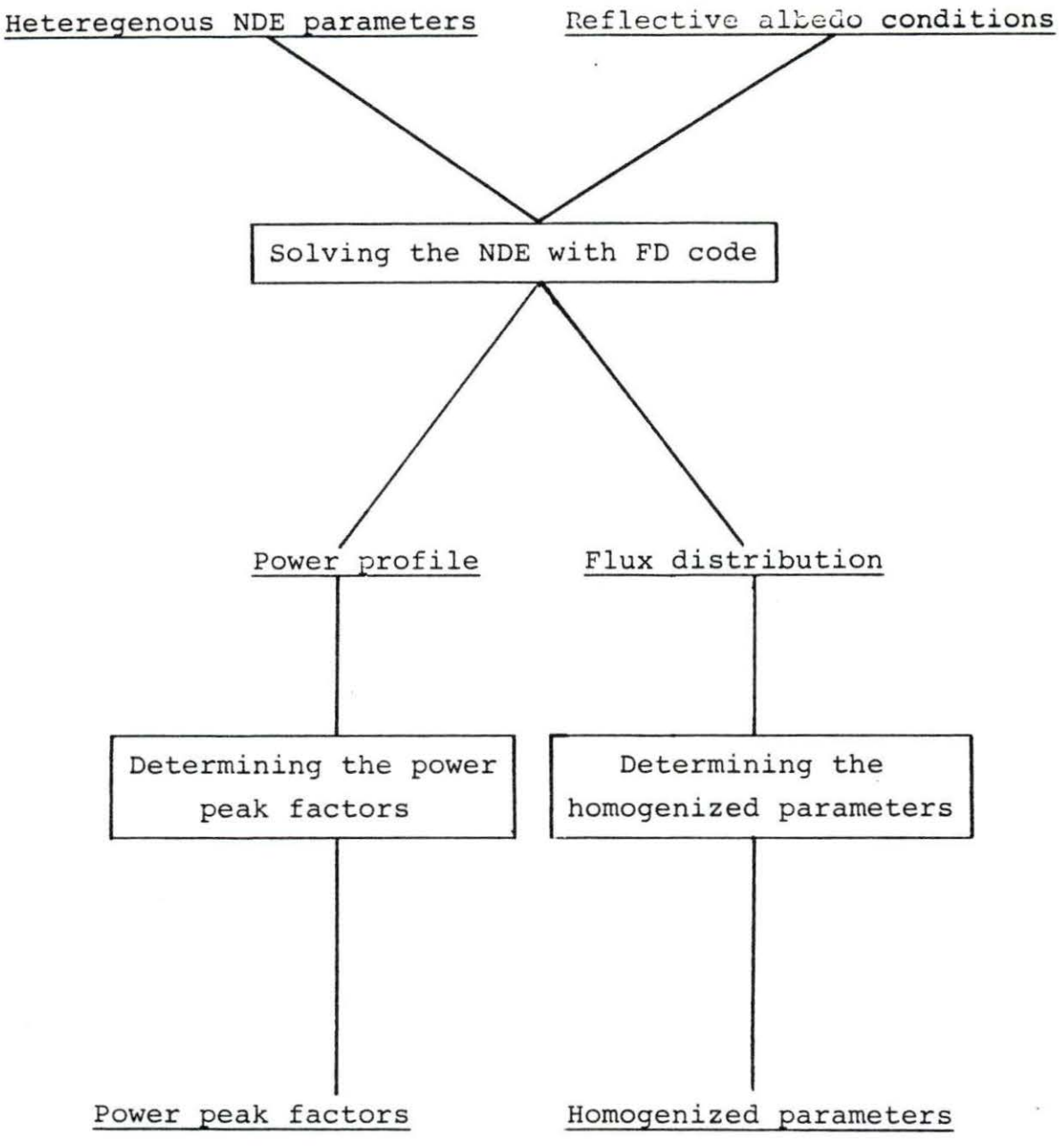

FIGURE 4. Flow diagram for preparing the homogenized neutronic parameters and the power peak factors

boundary condition for a single homogenized fuel assembly, the flux for that single fuel assembly should be in agreement with the one calculated for the coupled fuel assembly. In our case, typical interface albedo conditions for coupled fuel assemblies were used as the boundary conditions to simulate the fuel assemblies in a core. The finite difference code DTDMG was used to calculate the smooth power distribution for the homogenized fuel assembly.

Comparison of Superposed and Reference Solutions

The reference solution used for evaluating the performance of the method is obtained from an eigenvalue calculation with heterogeneous neutronic parameters by using the same albedo boundary conditions as was used in determining the smooth power profile for the homogenized fuel assembly. As in all other calculations, the reference solution was also determined by using the DTDMG code. Once the smooth power distributions for the homogenized fuel assembly were obtained for various albedo boundary conditions, they were normalized to the assembly average power given by the reference solution as below:

$$P_{nor}(x,y) = f.P_{hom}(x,y) \qquad (6\text{-}1)$$

where:

$$f = P_{ref}/P_{hom}$$

P_{ref} is average power given by the reference solution

P_{hom} is average power given by the smooth power distribution

The determination of the pin power distribution, the flow diagram for which is shown in Figure 5, is completed with multiplication of the smooth power distribution by the power peak factors in the following manner.

$$P_{pin}(x,y) = PPF(x,y).P_{nor}(x,y) \qquad (6\text{-}2)$$

where:

PPF(x,y) is power peak factor distribution

After the pin power distributions were determined, they were compared to the reference solutions to evaluate the performance of the method. This comparison is done by calculating the relative errors using the following criterion.

$$\text{Relative Error } \% = \frac{100}{P_{ref}(x,y)}[P_{pin}(x,y)-P_{ref}(x,y)] \qquad (6\text{-}3)$$

The relative errors calculated according to the above criterion are averaged over each cell shown in Figure 2 and an average cell error is determined.

The application of the method in this thesis has been based on a PWR fuel assembly which contains a 15X15 array of fuel pins, instrumentation sheath and control rod holes

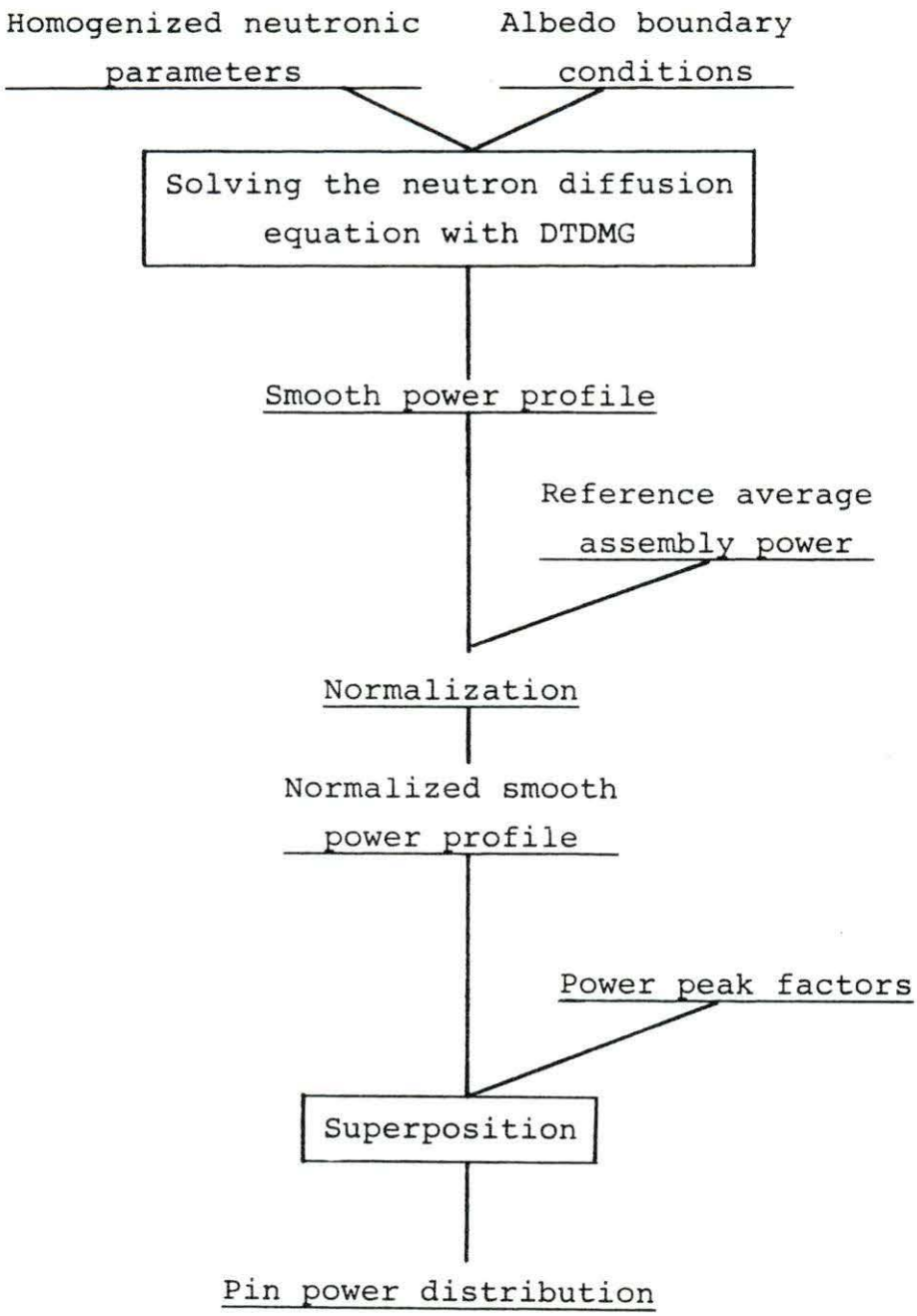

FIGURE 5. Flow diagram for determination of the pin power distribution by the superposition method

[14]. Parameters specifying the fuel assembly used in the calculations are listed in Table 1. The procedure of group cross section generation produces neutronic parameters for the all fuel cells. As a result of that, the fuel assembly with all the control rods fully withdrawn, can be represented as in Figure 2. The fuel, which was chosen to be uranium dioxide in this case, has an enrichment of 3 %. The cross sections used for calculations were generated by using the computer codes made available by the Nuclear Engineering Department of the Iowa State University [15].

TABLE 1. Some specifications of the fuel assembly

Diameter of the fuel pellets	0.93	cm
Thickness of the clad	0.06	cm
Outside diameter of the fuel rod	1.07	cm
Pitch	1.10	cm
Side length of the quarter assembly	21.40	cm
Side length of the assembly	42.90	cm

RESULTS

The structural materials, control rods, reflector around the core and the heterogeneous distribution of the fuel in the reactor causes a large number of the gradients in the flux distribution. The success of the superposition method depends on how well it can generate the pin power distribution under these large gradients. The method should be able to generate the pin power distributions with small errors for all cases. The gradients, which were used to test the performance of the superposition method, were imposed through the albedo boundary conditions. The albedo boundary condition can be defined as the ratio of incoming partial current to the outgoing partial current at the boundary.

$$\alpha = J_{in}/J_{out}$$

As can be seen from the definition above, the albedo can take various values as a function of the flux distribution in the close vicinity of the boundary. If the flux attains a higher value outside the boundary, this would cause the incoming partial current to be larger than the outgoing partial current. In such a case, the albedo takes values larger than 1.0. If the flux has a flat characteristic around the boundary, the incoming and the outgoing partial currents would be equal and the value of

the albedo would be 1.0. This case is usually known as the perfectly reflective boundary condition. The other alternative is that the albedo is less than 1.0. This takes place when the flux inside the boundary is higher than the flux outside the boundary. One extreme example for this case is to assume zero incoming partial current for which the albedo takes value of 0.0. In our applications, the albedo values have been chosen between 0.4 and 1.0.

In this thesis, the method of superposition was tested for 7 cases. In the first case, all the albedo conditions were chosen to be the reflective boundary conditions. Then the gradients imposed were increased in strength. Although the albedo conditions may vary along the sides of the fuel assembly, they were chosen to be constant for problem simplicity. Since the fast neutrons penetrate more than the thermal neutrons, the gradients imposed for the first group neutrons are larger than the second group neutrons. The albedo conditions used for the 7 cases are listed in Table 2

Figures 6-12 give the results for the cases tabulated in Table 2. The top numbers in each box give the average of the reference power for the corresponding fuel pin. The bottom numbers give the average of the percent errors for the same fuel pin. The boxes which contain the zeroes correspond to the water columns in the fuel assembly.

TABLE 2. Albedo boundary conditions for sample cases

Case	Group	Albedo Conditions			
		Inner	Outer	Lower	Upper
1	1	1.00	1.00	1.00	1.00
	2	1.00	1.00	1.00	1.00
2	1	0.80	0.90	0.95	0.85
	2	0.85	0.93	1.00	0.90
3	1	0.90	0.80	0.75	0.80
	2	0.93	0.88	0.80	0.85
4	1	1.00	0.50	1.00	0.70
	2	1.00	0.60	1.00	0.80
5	1	1.00	0.50	0.70	0.70
	2	1.00	0.60	0.80	0.80
6	1	0.70	0.50	0.50	0.70
	2	0.80	0.60	0.60	0.80
7	1	0.50	0.40	0.55	0.40
	2	0.60	0.50	0.65	0.50

1.70 0.03	1.73 0.03	1.75 0.03	1.77 0.03	1.77 0.03	1.78 0.02	1.78 0.02	1.77 0.02	1.78 0.02	1.78 0.02	1.77 0.02	1.76 0.01	1.75 0.01	1.73 0.01	1.70 0.01
1.73 0.03	1.78 0.03	1.84 0.03	1.84 0.03	1.85 0.03	1.88 0.03	1.86 0.02	1.83 0.02	1.86 0.02	1.88 0.02	1.85 0.02	1.84 0.01	1.84 0.01	1.78 0.01	1.73 0.01
1.75 0.03	1.84 0.03	0.00 0.00	1.93 0.03	1.95 0.03	0.00 0.00	1.98 0.02	1.95 0.02	1.98 0.02	0.00 0.00	1.95 0.02	1.93 0.01	0.00 0.00	1.84 0.01	1.75 0.01
1.77 0.03	1.84 0.03	1.93 0.03	1.97 0.03	2.01 0.03	2.02 0.03	2.00 0.02	0.00 0.00	2.00 0.02	2.02 0.02	2.01 0.01	1.97 0.01	1.93 0.01	1.84 0.01	1.76 0.01
1.77 0.03	1.85 0.03	1.95 0.03	2.01 0.03	0.00 0.00	1.97 0.02	1.93 0.02	1.94 0.02	1.93 0.02	1.97 0.01	0.00 0.00	2.01 0.01	1.95 0.01	1.85 0.01	1.77 0.01
1.78 0.03	1.88 0.03	0.00 0.00	2.02 0.03	1.97 0.02	1.90 0.02	1.86 0.02	1.86 0.02	1.86 0.01	1.90 0.01	1.97 0.01	2.02 0.01	0.00 0.00	1.88 0.01	1.78 0.01
1.78 0.03	1.86 0.03	1.98 0.03	2.00 0.02	1.93 0.02	1.86 0.02	1.87 0.02	1.89 0.02	1.87 0.01	1.86 0.01	1.93 0.01	2.00 0.01	1.98 0.01	1.86 0.01	1.78 0.01
1.77 0.02	1.83 0.02	1.95 0.02	0.00 0.00	1.94 0.02	1.86 0.02	1.89 0.02	0.00 0.00	1.89 0.01	1.86 0.01	1.94 0.01	0.00 0.00	1.95 0.01	1.83 0.00	1.77 0.00
1.78 0.02	1.86 0.02	1.98 0.02	2.00 0.02	1.93 0.02	1.86 0.02	1.87 0.01	1.89 0.01	1.87 0.01	1.86 0.01	1.93 0.01	2.00 0.01	1.98 0.00	1.86 0.00	1.78 0.00
1.78 0.02	1.88 0.02	0.00 0.00	2.02 0.02	1.97 0.02	1.90 0.01	1.86 0.01	1.86 0.01	1.86 0.01	1.90 0.01	1.97 0.01	2.02 0.00	0.00 0.00	1.88 0.00	1.78 0.00
1.77 0.02	1.85 0.02	1.95 0.02	2.01 0.02	0.00 0.00	1.97 0.01	1.93 0.01	1.94 0.01	1.93 0.01	1.97 0.01	0.00 0.00	2.01 0.00	1.95 0.00	1.85 0.00	1.77 0.00
1.76 0.02	1.84 0.02	1.93 0.02	1.97 0.02	2.01 0.02	2.02 0.01	2.00 0.01	0.00 0.00	2.00 0.01	2.02 0.01	2.01 0.00	1.97 0.00	1.93 0.00	1.84 0.00	1.76 0.00
1.75 0.02	1.84 0.02	0.00 0.00	1.93 0.02	1.95 0.01	0.00 0.00	1.98 0.01	1.95 0.01	1.98 0.01	0.00 0.00	1.95 0.00	1.93 0.00	0.00 0.00	1.84 0.00	1.75 0.00
1.73 0.02	1.78 0.02	1.84 0.02	1.84 0.01	1.85 0.01	1.88 0.01	1.86 0.01	1.83 0.01	1.86 0.01	1.88 0.00	1.85 0.00	1.84 0.00	1.84 0.00	1.78 0.00	1.73 0.00
1.70 0.02	1.73 0.01	1.75 0.01	1.76 0.01	1.77 0.01	1.78 0.01	1.78 0.01	1.77 0.01	1.78 0.00	1.78 0.00	1.77 0.00	1.76 0.00	1.75 0.00	1.73 0.00	1.70 0.00

FIGURE 6. The reference power profile and relative % error distribution for case 1

1.03 -1.15	1.14 -1.03	1.22 -0.95	1.28 -0.85	1.33 -0.77	1.36 -0.72	1.38 -0.66	1.40 -0.62	1.41 -0.64	1.42 -0.66	1.41 -0.66	1.40 -0.69	1.37 -0.73	1.32 -0.75	1.25 -0.82
1.11 -1.11	1.24 -0.94	1.35 -0.85	1.41 -0.74	1.46 -0.58	1.52 -0.50	1.53 -0.45	1.53 -0.42	1.56 -0.41	1.59 -0.42	1.56 -0.44	1.54 -0.49	1.52 -0.54	1.44 -0.57	1.34 -0.67
1.17 -1.10	1.34 -0.92	0.00 0.00	1.54 -0.67	1.60 -0.41	0.00 0.00	1.69 -0.21	1.70 -0.13	1.73 -0.16	0.00 0.00	1.71 -0.25	1.68 -0.35	0.00 0.00	1.55 -0.46	1.42 -0.57
1.22 -1.05	1.38 -0.86	1.53 -0.72	1.62 -0.45	1.70 -0.16	1.75 -0.03	1.77 0.10	0.00 0.00	1.81 0.12	1.82 0.09	1.82 0.03	1.77 -0.11	1.71 -0.26	1.59 -0.33	1.47 -0.45
1.25 -1.00	1.42 -0.75	1.58 -0.54	1.69 -0.21	0.00 0.00	1.75 0.27	1.74 0.38	1.77 0.37	1.78 0.38	1.82 0.37	0.00 0.00	1.85 0.13	1.77 -0.03	1.65 -0.17	1.52 -0.36
1.29 -0.98	1.47 -0.70	0.00 0.00	1.73 -0.11	1.74 0.26	1.72 0.42	1.71 0.49	1.74 0.50	1.75 0.50	1.80 0.47	1.86 0.39	1.89 0.23	0.00 0.00	1.70 -0.09	1.56 -0.29
1.30 -0.92	1.48 -0.66	1.66 -0.35	1.75 0.03	1.73 0.36	1.71 0.50	1.75 0.52	1.80 0.53	1.79 0.53	1.79 0.54	1.85 0.50	1.91 0.35	1.86 0.15	1.71 -0.03	1.58 -0.22
1.32 -0.88	1.48 -0.62	1.66 -0.27	0.00 0.00	1.76 0.36	1.73 0.51	1.80 0.54	0.00 0.00	1.84 0.55	1.81 0.56	1.88 0.51	0.00 0.00	1.86 0.23	1.71 0.03	1.59 -0.17
1.33 -0.89	1.51 -0.60	1.70 -0.28	1.79 0.07	1.77 0.39	1.75 0.53	1.79 0.56	1.84 0.56	1.83 0.57	1.83 0.58	1.90 0.53	1.96 0.42	1.91 0.25	1.75 0.06	1.62 -0.15
1.35 -0.89	1.54 -0.58	0.00 0.00	1.82 0.08	1.83 0.43	1.81 0.53	1.80 0.59	1.82 0.60	1.84 0.60	1.89 0.60	1.95 0.59	1.99 0.45	0.00 0.00	1.79 0.09	1.63 -0.13
1.35 -0.85	1.53 -0.55	1.70 -0.30	1.82 0.08	0.00 0.00	1.88 0.51	1.87 0.62	1.91 0.64	1.92 0.63	1.97 0.63	0.00 0.00	1.99 0.48	1.91 0.30	1.77 0.12	1.63 -0.10
1.34 -0.82	1.52 -0.51	1.68 -0.26	1.79 0.05	1.88 0.36	1.93 0.50	1.95 0.62	0.00 0.00	2.00 0.65	2.02 0.66	2.01 0.61	1.96 0.49	1.89 0.33	1.76 0.15	1.63 -0.08
1.34 -0.79	1.52 -0.46	0.00 0.00	1.75 0.02	1.83 0.35	0.00 0.00	1.93 0.57	1.93 0.63	1.97 0.64	0.00 0.00	1.95 0.60	1.91 0.47	0.00 0.00	1.76 0.17	1.62 -0.07
1.31 -0.70	1.47 -0.38	1.60 -0.15	1.67 0.08	1.73 0.32	1.80 0.45	1.81 0.52	1.81 0.58	1.85 0.60	1.88 0.60	1.85 0.56	1.82 0.46	1.80 0.35	1.70 0.19	1.59 -0.03
1.29 -0.61	1.41 -0.30	1.52 -0.07	1.59 0.14	1.65 0.31	1.70 0.42	1.73 0.50	1.74 0.55	1.76 0.57	1.77 0.57	1.76 0.54	1.74 0.47	1.71 0.37	1.64 0.22	1.56 0.02

FIGURE 7. The reference power profile and relative % error distribution for case 2

1.29 -0.77	1.36 -0.72	1.42 -0.71	1.45 -0.67	1.47 -0.64	1.48 -0.65	1.48 -0.62	1.47 -0.60	1.46 -0.65	1.45 -0.71	1.42 -0.74	1.38 -0.81	1.33 -0.90	1.25 -0.95	1.16 -1.05
1.42 -0.52	1.52 -0.42	1.61 -0.39	1.63 -0.35	1.66 -0.29	1.69 -0.27	1.67 -0.26	1.64 -0.27	1.65 -0.30	1.66 -0.35	1.60 -0.41	1.56 -0.55	1.51 -0.66	1.40 -0.73	1.27 -0.89
1.51 -0.34	1.65 -0.23	0.00 0.00	1.80 -0.10	1.84 0.01	0.00 0.00	1.87 0.10	1.84 0.13	1.85 0.05	0.00 0.00	1.77 -0.14	1.72 -0.36	0.00 0.00	1.52 -0.61	1.36 -0.79
1.58 -0.18	1.71 -0.04	1.83 0.05	1.90 0.23	1.96 0.38	1.97 0.43	1.96 0.48	0.00 0.00	1.94 0.45	1.93 0.32	1.89 0.21	1.81 -0.06	1.72 -0.33	1.57 -0.47	1.42 -0.68
1.62 -0.06	1.76 0.16	1.90 0.33	1.98 0.52	0.00 0.00	1.97 0.77	1.92 0.78	1.93 0.76	1.90 0.76	1.92 0.67	0.00 0.00	1.89 0.24	1.78 -0.07	1.62 -0.31	1.46 -0.59
1.65 0.01	1.81 0.24	0.00 0.00	2.01 0.64	1.99 0.81	1.92 0.88	1.88 0.90	1.87 0.89	1.86 0.88	1.88 0.81	1.92 0.67	1.92 0.35	0.00 0.00	1.67 -0.24	1.48 -0.55
1.66 0.05	1.80 0.28	1.96 0.50	2.01 0.72	1.95 0.88	1.89 0.92	1.90 0.91	1.92 0.90	1.88 0.89	1.85 0.86	1.88 0.74	1.92 0.44	1.84 0.10	1.66 -0.21	1.49 -0.50
1.65 0.07	1.77 0.30	1.93 0.55	0.00 0.00	1.96 0.88	1.89 0.92	1.93 0.91	0.00 0.00	1.90 0.89	1.84 0.86	1.89 0.73	0.00 0.00	1.81 0.16	1.63 -0.19	1.48 -0.48
1.64 0.03	1.78 0.25	1.94 0.46	1.99 0.69	1.93 0.86	1.87 0.91	1.88 0.90	1.90 0.89	1.86 0.88	1.83 0.85	1.86 0.73	1.90 0.43	1.82 0.07	1.64 -0.23	1.47 -0.52
1.62 -0.05	1.77 0.17	0.00 0.00	1.97 0.55	1.94 0.74	1.88 0.83	1.84 0.86	1.83 0.85	1.82 0.84	1.84 0.76	1.87 0.61	1.88 0.28	0.00 0.00	1.63 -0.30	1.45 -0.59
1.57 -0.16	1.70 0.05	1.84 0.21	1.92 0.39	0.00 0.00	1.90 0.68	1.86 0.69	1.86 0.67	1.84 0.67	1.86 0.58	0.00 0.00	1.83 0.12	1.72 -0.17	1.57 -0.39	1.41 -0.66
1.51 -0.32	1.63 -0.22	1.76 -0.17	1.82 0.01	1.87 0.17	1.89 0.22	1.87 0.29	0.00 0.00	1.85 0.26	1.84 0.12	1.81 0.01	1.74 -0.25	1.65 -0.51	1.51 -0.61	1.36 -0.77
1.43 -0.52	1.56 -0.45	0.00 0.00	1.70 -0.39	1.74 -0.29	0.00 0.00	1.77 -0.18	1.74 -0.14	1.74 -0.22	0.00 0.00	1.67 -0.42	1.62 -0.62	0.00 0.00	1.44 -0.78	1.28 -0.92
1.31 -0.72	1.41 -0.67	1.49 -0.68	1.51 -0.66	1.54 -0.62	1.57 -0.61	1.55 -0.60	1.53 -0.60	1.53 -0.63	1.54 -0.67	1.49 -0.72	1.44 -0.83	1.40 -0.90	1.30 -0.92	1.18 -1.03
1.17 -1.00	1.23 -0.99	1.28 -1.03	1.31 -1.00	1.33 -0.99	1.34 -1.01	1.34 -0.97	1.33 -0.95	1.32 -0.99	1.31 -1.05	1.28 -1.06	1.25 -1.11	1.20 -1.17	1.13 -1.17	1.05 -1.21

FIGURE 8. The reference power profile and relative % error distribution for case 3

1.07 -0.88	1.08 -1.00	1.08 -1.14	1.07 -1.20	1.05 -1.26	1.03 -1.32	0.99 -1.30	0.94 -1.27	0.90 -1.30	0.85 -1.36	0.79 -1.38	0.72 -1.44	0.64 -1.48	0.55 -1.43	0.43 -1.39
1.21 -0.48	1.25 -0.59	1.27 -0.72	1.25 -0.82	1.23 -0.94	1.22 -0.97	1.16 -1.00	1.09 -1.03	1.05 -1.08	1.01 -1.14	0.92 -1.20	0.84 -1.42	0.75 -1.49	0.63 -1.47	0.49 -1.49
1.34 -0.13	1.40 -0.26	0.00 0.00	1.43 -0.49	1.41 -0.63	0.00 0.00	1.34 -0.63	1.26 -0.61	1.21 -0.74	0.00 0.00	1.05 -1.03	0.96 -1.43	0.00 0.00	0.71 -1.56	0.54 -1.61
1.43 0.19	1.49 0.09	1.54 -0.03	1.55 -0.06	1.55 -0.09	1.50 -0.11	1.44 -0.18	0.00 0.00	1.31 -0.20	1.24 -0.48	1.15 -0.67	1.04 -1.15	0.92 -1.53	0.76 -1.59	0.58 -1.64
1.52 0.49	1.58 0.51	1.64 0.52	1.67 0.39	0.00 0.00	1.55 0.38	1.46 0.26	1.40 0.25	1.32 0.29	1.27 0.05	0.00 0.00	1.12 -0.79	0.98 -1.32	0.80 -1.52	0.62 -1.66
1.60 0.73	1.68 0.73	0.00 0.00	1.75 0.58	1.67 0.48	1.56 0.50	1.47 0.48	1.41 0.47	1.33 0.48	1.28 0.33	1.24 0.04	1.17 -0.65	0.00 0.00	0.85 -1.50	0.65 -1.70
1.65 0.91	1.72 0.91	1.81 0.88	1.80 0.82	1.69 0.70	1.59 0.61	1.54 0.54	1.49 0.53	1.39 0.53	1.30 0.47	1.26 0.21	1.20 -0.43	1.07 -1.08	0.87 -1.49	0.67 -1.67
1.70 1.04	1.75 1.07	1.85 1.02	0.00 0.00	1.76 0.74	1.64 0.63	1.61 0.54	0.00 0.00	1.46 0.54	1.35 0.47	1.31 0.17	0.00 0.00	1.09 -0.98	0.89 -1.49	0.69 -1.65
1.76 1.15	1.83 1.19	1.92 1.16	1.92 0.97	1.81 0.75	1.69 0.64	1.64 0.57	1.59 0.55	1.49 0.55	1.39 0.48	1.34 0.20	1.28 -0.42	1.14 -1.05	0.93 -1.48	0.71 -1.71
1.81 1.27	1.90 1.30	0.00 0.00	1.98 1.16	1.89 0.91	1.77 0.74	1.67 0.63	1.60 0.62	1.51 0.61	1.46 0.47	1.40 0.26	1.32 -0.44	0.00 0.00	0.97 -1.47	0.74 -1.76
1.83 1.36	1.91 1.39	1.98 1.42	2.01 1.28	0.00 0.00	1.87 0.91	1.77 0.70	1.70 0.70	1.60 0.68	1.54 0.37	0.00 0.00	1.35 -0.47	1.18 -1.16	0.97 -1.46	0.75 -1.71
1.85 1.43	1.92 1.49	1.99 1.56	2.00 1.45	2.00 1.25	1.94 1.12	1.86 0.87	0.00 0.00	1.69 0.70	1.60 0.37	1.49 0.10	1.34 -0.51	1.18 -1.06	0.98 -1.37	0.75 -1.66
1.86 1.45	1.95 1.49	0.00 0.00	1.98 1.53	1.96 1.33	0.00 0.00	1.86 1.03	1.76 0.88	1.69 0.67	0.00 0.00	1.46 0.18	1.33 -0.53	0.00 0.00	0.99 -1.24	0.76 -1.61
1.85 1.42	1.90 1.45	1.94 1.48	1.90 1.45	1.87 1.30	1.85 1.19	1.76 1.04	1.66 0.89	1.60 0.68	1.53 0.45	1.40 0.18	1.27 -0.36	1.14 -0.75	0.96 -1.06	0.75 -1.44
1.83 1.39	1.85 1.41	1.85 1.42	1.83 1.37	1.80 1.27	1.76 1.15	1.69 0.99	1.61 0.85	1.54 0.69	1.45 0.45	1.34 0.16	1.22 -0.20	1.09 -0.57	0.93 -0.92	0.74 -1.28

FIGURE 9. The reference power profile and relative % error distribution for case 4

1.29 -0.47	1.30 -0.60	1.31 -0.75	1.29 -0.81	1.27 -0.89	1.24 -0.98	1.19 -1.00	1.14 -0.99	1.08 -1.05	1.02 -1.15	0.95 -1.22	0.86 -1.33	0.77 -1.42	0.66 -1.43	0.52 -1.44
1.45 0.08	1.50 -0.03	1.53 -0.16	1.50 -0.27	1.48 -0.42	1.46 -0.49	1.39 -0.56	1.31 -0.63	1.26 -0.72	1.20 -0.82	1.10 -0.94	1.01 -1.24	0.90 -1.39	0.76 -1.43	0.59 -1.53
1.59 0.53	1.66 0.42	0.00 0.00	1.70 0.20	1.68 0.02	0.00 0.00	1.59 -0.08	1.50 -0.11	1.44 -0.29	0.00 0.00	1.25 -0.68	1.14 -1.19	0.00 0.00	0.84 -1.50	0.65 -1.64
1.68 0.92	1.75 0.84	1.81 0.75	1.82 0.70	1.82 0.61	1.77 0.53	1.69 0.40	0.00 0.00	1.54 0.30	1.45 -0.05	1.35 -0.29	1.22 -0.86	1.07 -1.36	0.89 -1.51	0.68 -1.65
1.75 1.22	1.82 1.26	1.90 1.28	1.93 1.15	0.00 0.00	1.79 1.00	1.68 0.81	1.62 0.77	1.53 0.78	1.47 0.48	0.00 0.00	1.29 -0.49	1.12 -1.14	0.93 -1.43	0.71 -1.66
1.81 1.42	1.90 1.45	0.00 0.00	1.98 1.32	1.89 1.14	1.77 1.08	1.66 1.00	1.59 0.97	1.51 0.95	1.45 0.76	1.40 0.45	1.32 -0.32	0.00 0.00	0.96 -1.39	0.73 -1.68
1.83 1.52	1.90 1.55	2.00 1.54	1.99 1.43	1.87 1.26	1.75 1.13	1.70 1.02	1.65 0.98	1.54 0.96	1.44 0.87	1.39 0.57	1.33 -0.15	1.18 -0.88	0.96 -1.38	0.74 -1.63
1.83 1.55	1.88 1.61	1.98 1.59	0.00 0.00	1.89 1.29	1.76 1.14	1.73 1.02	0.00 0.00	1.57 0.97	1.45 0.87	1.40 0.53	0.00 0.00	1.17 -0.77	0.96 -1.37	0.74 -1.59
1.83 1.51	1.90 1.55	2.00 1.53	1.99 1.43	1.87 1.25	1.75 1.13	1.70 1.02	1.65 0.98	1.54 0.96	1.44 0.87	1.39 0.56	1.33 -0.15	1.18 -0.88	0.96 -1.38	0.74 -1.64
1.81 1.41	1.90 1.44	0.00 0.00	1.98 1.31	1.89 1.13	1.77 1.07	1.66 0.99	1.59 0.97	1.51 0.94	1.45 0.75	1.40 0.44	1.32 -0.33	0.00 0.00	0.96 -1.40	0.73 -1.69
1.75 1.21	1.82 1.24	1.90 1.27	1.92 1.13	0.00 0.00	1.79 0.98	1.68 0.80	1.62 0.76	1.53 0.77	1.47 0.47	0.00 0.00	1.29 -0.49	1.12 -1.15	0.93 -1.43	0.71 -1.66
1.68 0.90	1.75 0.82	1.81 0.74	1.82 0.69	1.82 0.59	1.77 0.52	1.69 0.39	0.00 0.00	1.54 0.28	1.45 -0.06	1.35 -0.30	1.22 -0.87	1.07 -1.36	0.89 -1.52	0.68 -1.66
1.59 0.52	1.66 0.40	0.00 0.00	1.69 0.18	1.67 0.00	0.00 0.00	1.59 -0.09	1.50 -0.12	1.44 -0.30	0.00 0.00	1.25 -0.69	1.13 -1.20	0.00 0.00	0.84 -1.51	0.65 -1.65
1.45 0.06	1.50 -0.05	1.53 -0.17	1.50 -0.29	1.48 -0.43	1.46 -0.51	1.39 -0.57	1.31 -0.64	1.26 -0.73	1.20 -0.83	1.10 -0.95	1.01 -1.25	0.90 -1.39	0.76 -1.44	0.59 -1.54
1.29 -0.49	1.30 -0.62	1.31 -0.76	1.29 -0.83	1.27 -0.91	1.24 -0.99	1.19 -1.01	1.14 -1.00	1.08 -1.07	1.02 -1.16	0.95 -1.23	0.86 -1.34	0.77 -1.43	0.66 -1.44	0.52 -1.44

FIGURE 10. The reference power profile and relative % error distribution for case 5

1.04 -1.24	1.18 -1.08	1.28 -0.98	1.35 -0.83	1.39 -0.72	1.42 -0.69	1.41 -0.62	1.39 -0.58	1.36 -0.65	1.32 -0.77	1.25 -0.88	1.16 -1.05	1.05 -1.25	0.90 -1.35	0.72 -1.48
1.18 -1.08	1.35 -0.78	1.50 -0.61	1.56 -0.41	1.62 -0.19	1.67 -0.10	1.65 -0.06	1.60 -0.05	1.59 -0.14	1.55 -0.25	1.45 -0.43	1.34 -0.82	1.22 -1.09	1.03 -1.27	0.81 -1.54
1.28 -0.98	1.50 -0.61	0.00 0.00	1.75 -0.07	1.82 0.30	0.00 0.00	1.87 0.55	1.83 0.62	1.81 0.45	0.00 0.00	1.63 -0.01	1.51 -0.65	0.00 0.00	1.14 -1.28	0.88 -1.62
1.35 -0.83	1.56 -0.41	1.75 -0.07	1.87 0.43	1.96 0.89	1.99 1.06	1.98 1.17	0.00 0.00	1.91 1.11	1.85 0.80	1.76 0.50	1.61 -0.21	1.44 -0.88	1.20 -1.24	0.93 -1.59
1.39 -0.72	1.62 -0.19	1.82 0.30	1.96 0.89	0.00 0.00	2.00 1.59	1.95 1.65	1.94 1.64	1.88 1.63	1.86 1.36	0.00 0.00	1.69 0.23	1.49 -0.61	1.24 -1.12	0.96 -1.57
1.42 -0.68	1.67 -0.09	0.00 0.00	1.99 1.06	2.00 1.59	1.95 1.77	1.91 1.83	1.89 1.83	1.84 1.80	1.81 1.63	1.78 1.30	1.71 0.42	0.00 0.00	1.27 -1.06	0.98 -1.59
1.41 -0.62	1.65 -0.06	1.87 0.55	1.98 1.17	1.95 1.65	1.91 1.83	1.92 1.82	1.93 1.80	1.85 1.79	1.78 1.72	1.75 1.38	1.70 0.57	1.53 -0.32	1.26 -1.04	0.97 -1.52
1.39 -0.58	1.60 -0.05	1.83 0.62	0.00 0.00	1.94 1.64	1.89 1.83	1.93 1.80	0.00 0.00	1.86 1.78	1.75 1.72	1.73 1.35	0.00 0.00	1.49 -0.21	1.23 -1.02	0.96 -1.45
1.36 -0.65	1.59 -0.13	1.81 0.45	1.91 1.12	1.88 1.63	1.84 1.81	1.85 1.79	1.86 1.78	1.79 1.76	1.71 1.70	1.68 1.37	1.64 0.55	1.48 -0.37	1.22 -1.06	0.94 -1.50
1.32 -0.77	1.55 -0.25	0.00 0.00	1.85 0.80	1.86 1.37	1.81 1.63	1.78 1.72	1.75 1.72	1.71 1.70	1.69 1.51	1.66 1.12	1.59 0.25	0.00 0.00	1.19 -1.10	0.91 -1.57
1.25 -0.87	1.45 -0.42	1.63 0.00	1.76 0.50	0.00 0.00	1.78 1.30	1.75 1.38	1.73 1.35	1.68 1.37	1.66 1.13	0.00 0.00	1.51 -0.03	1.34 -0.77	1.11 -1.19	0.86 -1.56
1.16 -1.05	1.34 -0.81	1.51 -0.64	1.61 -0.20	1.69 0.24	1.71 0.42	1.70 0.57	0.00 0.00	1.64 0.55	1.59 0.25	1.51 -0.03	1.38 -0.66	1.23 -1.23	1.03 -1.41	0.80 -1.60
1.05 -1.24	1.22 -1.09	0.00 0.00	1.44 -0.88	1.49 -0.61	0.00 0.00	1.53 -0.32	1.49 -0.21	1.48 -0.37	0.00 0.00	1.34 -0.77	1.23 -1.23	0.00 0.00	0.94 -1.50	0.72 -1.63
0.90 -1.35	1.03 -1.27	1.14 -1.28	1.20 -1.23	1.24 -1.11	1.27 -1.06	1.26 -1.03	1.23 -1.02	1.22 -1.06	1.19 -1.10	1.11 -1.19	1.03 -1.41	0.94 -1.50	0.79 -1.48	0.62 -1.53
0.72 -1.48	0.81 -1.53	0.88 -1.62	0.93 -1.59	0.96 -1.57	0.98 -1.59	0.97 -1.52	0.96 -1.45	0.94 -1.50	0.91 -1.56	0.86 -1.56	0.80 -1.60	0.72 -1.63	0.62 -1.53	0.50 -1.44

FIGURE 11. The reference power profile and relative % error distribution for case 6

0.51 -1.53	0.64 -1.64	0.74 -1.76	0.81 -1.73	0.86 -1.69	0.89 -1.70	0.91 -1.62	0.90 -1.54	0.89 -1.60	0.87 -1.68	0.82 -1.66	0.75 -1.70	0.67 -1.72	0.57 -1.59	0.43 -1.44
0.67 -1.61	0.86 -1.54	1.00 -1.55	1.09 -1.45	1.17 -1.22	1.23 -1.12	1.23 -1.07	1.22 -1.04	1.21 -1.07	1.19 -1.12	1.11 -1.22	1.02 -1.49	0.92 -1.59	0.76 -1.56	0.57 -1.59
0.80 -1.69	1.04 -1.50	0.00 0.00	1.34 -1.12	1.44 -0.63	0.00 0.00	1.53 -0.17	1.52 0.00	1.51 -0.19	0.00 0.00	1.37 -0.67	1.26 -1.23	0.00 0.00	0.92 -1.59	0.68 -1.72
0.90 -1.61	1.16 -1.32	1.38 -1.04	1.53 -0.35	1.65 0.38	1.71 0.70	1.73 0.98	0.00 0.00	1.70 0.98	1.66 0.63	1.57 0.28	1.43 -0.51	1.26 -1.23	1.03 -1.49	0.76 -1.70
0.98 -1.53	1.26 -0.99	1.50 -0.40	1.68 0.47	0.00 0.00	1.80 1.80	1.79 2.00	1.80 1.98	1.76 2.00	1.74 1.73	0.00 0.00	1.58 0.28	1.38 -0.67	1.12 -1.23	0.82 -1.67
1.04 -1.52	1.35 -0.86	0.00 0.00	1.78 0.83	1.83 1.81	1.83 2.24	1.83 2.42	1.83 2.43	1.80 2.42	1.78 2.19	1.75 1.73	1.67 0.62	0.00 0.00	1.20 -1.13	0.87 -1.69
1.07 -1.43	1.38 -0.79	1.67 0.10	1.83 1.18	1.86 2.10	1.86 2.45	1.91 2.48	1.94 2.48	1.88 2.47	1.80 2.42	1.77 2.01	1.71 0.98	1.52 -0.19	1.23 -1.08	0.90 -1.62
1.09 -1.36	1.39 -0.74	1.68 0.28	0.00 0.00	1.91 2.08	1.90 2.47	1.97 2.48	0.00 0.00	1.94 2.47	1.84 2.43	1.82 1.98	0.00 0.00	1.54 -0.01	1.23 -1.05	0.92 -1.56
1.10 -1.45	1.41 -0.78	1.70 0.12	1.87 1.19	1.90 2.09	1.91 2.45	1.95 2.48	1.98 2.48	1.92 2.47	1.85 2.42	1.81 2.00	1.75 0.98	1.56 -0.18	1.25 -1.08	0.92 -1.65
1.09 -1.55	1.41 -0.84	0.00 0.00	1.86 0.93	1.92 1.91	1.92 2.29	1.92 2.46	1.92 2.48	1.89 2.45	1.86 2.24	1.83 1.81	1.75 0.71	0.00 0.00	1.26 -1.13	0.92 -1.74
1.05 -1.56	1.35 -0.96	1.61 -0.32	1.81 0.62	0.00 0.00	1.94 1.92	1.93 2.12	1.94 2.12	1.90 2.12	1.88 1.84	0.00 0.00	1.69 0.41	1.48 -0.62	1.20 -1.23	0.88 -1.72
0.99 -1.64	1.28 -1.24	1.52 -0.84	1.69 -0.08	1.82 0.68	1.89 1.00	1.91 1.28	0.00 0.00	1.88 1.27	1.83 0.92	1.74 0.56	1.58 -0.28	1.39 -1.08	1.13 -1.44	0.84 -1.76
0.92 -1.73	1.19 -1.40	0.00 0.00	1.54 -0.79	1.64 -0.19	0.00 0.00	1.76 0.26	1.74 0.43	1.73 0.24	0.00 0.00	1.57 -0.27	1.44 -0.95	0.00 0.00	1.05 -1.54	0.77 -1.80
0.81 -1.68	1.03 -1.47	1.20 -1.36	1.31 -1.15	1.40 -0.82	1.47 -0.68	1.48 -0.61	1.46 -0.56	1.46 -0.62	1.43 -0.71	1.33 -0.86	1.23 -1.23	1.10 -1.45	0.91 -1.53	0.68 -1.68
0.67 -1.66	0.83 -1.65	0.95 -1.66	1.04 -1.54	1.11 -1.43	1.16 -1.39	1.18 -1.29	1.17 -1.22	1.16 -1.29	1.13 -1.39	1.06 -1.43	0.98 -1.54	0.87 -1.65	0.73 -1.62	0.56 -1.59

FIGURE 12. The reference power profile and relative % error distribution for case 7

Since we tried to determine the pin power distribution, our main concern is the magnitudes of the errors which arise in that estimation process. If the maximum (+) and (-) errors are studied in Figures 6-12, we see that (+) maximum errors vary to 2.48 % while (-) maximum errors vary to -1.80 %. The maximum (+) and (-) errors are tabulated in Table 3 for all cases.

TABLE 3. The maximum relative % errors for the sample cases

Case	Maximum (+) % Error	Maximum (-) % Error
1	Negligible	Negligible
2	0.66	-1.15
3	0.92	-1.21
4	1.56	-1.76
5	1.61	-1.69
6	1.83	-1.63
7	2.48	-1.80

Some other observations can be made upon the positions of the maximum errors. The (+) errors are observed to be positioned where the power levels are higher while the (-) errors are usually located where the power levels are lower. The maximum errors are attained near the power peaks for the (+) errors and the maximums for the (-) errors are observed near the power troughs. In other words, the method estimates the power peaks in a conservative manner.

TABLE 4. Comparison of the minimum and the maximum power levels in the fuel assembly with the power levels in the cells with the maximum relative errors

Case	Maximum power	Minimum power	Power in the cell of maximum %	
			(+) error	(-) error
2	2.02	1.03	2.02	1.03
3	2.01	1.03	1.89	1.05
4	2.01	0.43	1.99	0.74
5	2.00	0.52	1.88	0.73
6	2.00	0.50	1.91	0.72
7	1.97	0.43	1.95	0.77

Another useful set of information is obtained, if the differences in the temperatures induced by the inaccuricies in the power calculations are estimated. The fuel pin centerline temperature differences (°C) induced by the (+) relative errors, which were calculated by using the formalism in the Appendix, are listed in Table 5.

TABLE 5. Differences in the fuel pin centerline temperatures induced by the (+) relative errors in the power calculations

Case	(+) Relative % error	∇T (°C) induced by error
2	0.66	9
3	0.92	13
4	1.56	22
5	1.61	22
6	1.83	25
7	2.48	34

CONCLUSIONS

In this thesis, a method of superposition was applied to determine the pin power distributions in PWR fuel assemblies which contain water regions. In this method, fuel assemblies were homogenized by weighting the space dependent neutronic parameters with flux computed for a fuel assembly with perfectly reflective boundary conditions. Typical interface currents were then used to generate internal flux distributions within a fuel assembly, and the power peak factors from the initial calculation with reflective boundary conditions used to get a final estimate of local pin power distribution. The pin power distributions estimated by the method of superposition were compared to reference power profiles to determine how the method performs under various conditions. One important point in evaluating the results is that the method should estimate the pin power distribution in a conservative manner. In other words, the method should overestimate the power levels in the fuel assembly to satisfy the safety considerations. If we look at the Table 3, we see that the method overestimates the power at some locations while it underestimates the power at some other locations. As a consequence of this, the locations of the underestimated power levels become significant. If we study Table 4, we see that the power is underestimated where the power levels

are far below the maximum power level. Since the maximum power is chosen to satisfy the constraints on the maximum power level, the power levels where they are underestimated by the method are very unlikely to approach the maximum power level constraints. As a result of this discussion, we can say that the method satisfies the conditions imposed by the safety considerations.

Another important point the method should satisfy is that the errors arising in the estimation process should not be very large. Since the maximum power in the reactor is fixed to satisfy the safety considerations, the actual maximum power would become lower as the errors in estimating the power levels become larger. This is not a desirable result since it reduces the efficiency of a reactor. If we look at the Table 3, we see that the largest (+) relative error is 2.48 % while the maximum (-) relative error ever reached in 7 cases is - 1.80 %. Although these magnititutes seem to be small, we can have a clearer idea if we look at fuel pin centerline temperature differences induced by these errors. As was discussed in the previous paragraph, (-) relative errors lose their importance since they are positioned where the power levels are low. Therefore, we look at the temperature differences caused by the (+) relative errors. As we can see from the Table 5, even under very sharp gradients, the temperatures can be estimated with

a difference of 34 °C and this difference is at a manageable level when compared to the maximum permissible level fuel temperatures about 2000 °C. As a result, we can say that the superposition method is succesful in determining pin power distribution.

BIBLIOGRAPHY

1. A. Mueller and M. R. Wagner, Trans. Am. Nucl. Soc. 15, 280 (1972).

2. M. R. Wagner and K. Koebke, in Proceedings of ANS Topical Meeting on Advances in Reactor Computations, Utah (1983), Vol. II, p. 941.

3. K. S. Smith, A. F. Henry and R. A. Loretz, in Proceedings of ANS Topical Meeting, Idaho (1980), p. 24.

4. A. Y. Cheng, C. L. Hoxie and A. F. Henry, in Proceedings of International Topical Meeting on Advance in Mathematical Methods for the Solution of Nuclear Engineering Problems, Munich (1981), Vol. II, p. 3.

5. F. Nissen, in Proceedings of ANS Topical Meeting on Advances in Reactor Computations, Utah (1983), Vol. I, p. 380.

6. K. Koebke and M. R. Wagner, Atomkernenergie 30, 136 (1977).

7. C. L. Hoxie and A. F. Henry, Trans. Am. Nucl. Soc. 22, 250 (1975).

8. H. J. Fenech and A. F. Rohach, EPRI Project Final Report RP 1251-1, (1980).

9. H. S. Khalil, P. J. Finck and A. F. Henry, in Proceedings of ANS Topical Meeting on Advances in Reactor Compututations, Utah (1983), Vol. I, p. 367.

10. A. F. Henry, Nuclear Reactor Analysis, The MIT Press, Cambridge, Massachusettes (1975).

11. H. Finnemann, F. Bennewitz and M. R. Wagner, Atomkernenergie 30, 123 (1977).

12. F. Bennewitz, H. Finnemann and H. Moldaschl, USAEC Document CONF-750413; in Proceedings of Conference on Computational Methods in Nuclear Engineering, South Carolina (1975), Vol. I, p. 99.

13. F. Bennewitz, H. Finnemann and M. R. Wagner, Trans. Am. Nucl. Soc. 22, 250 (1975).

14. A. F. Henry and B. A. Worley, EPRI Final Report 305 (1975).

15. A. F. Rohach, private communication, The Iowa State University, Department of Nuclear Engineering, 1985.

ACKNOWLEDGMENTS

I want to thank my major professor Dr. Alfred F. Rohach and the faculty of the Nuclear Engineering Department for their help and their contribution to my graduate study. I am also grateful for the financial support provided by the people of my country.

APPENDIX

If the fuel rods are assumed to have circular symmetry, a 2-D problem can be reduced to a 1-D problen and for such a case the heat conduction equation can be written as below:

$$\frac{1}{r}[\frac{d}{dr}(\frac{dT}{dr})]+\frac{q}{k} = 0 \qquad \text{(A-1)}$$

where:

q power density, watt/cm^3

k thermal conductivity coefficient, watt/cm °C

For the homogenous material properties and the power density, this differential equation can be solved analytically. If we assume that the surface temperature of the fuel pellets and the inner surface temperature of the clad are the same and the outer surface temperature of the clad is insensitive to small changes in the power density, we can calculate the temperature change at the centerline of the fuel pellets. This temperature change induced by the change in the power density is given as:

$$\nabla T = R^2[\frac{1}{4k_f}+\frac{1}{2k_c}+\ln(\frac{R+c}{R})](q_B-q_A) \qquad \text{(A-2)}$$

where:

∇T change in temperature, °C

R radius of the fuel pellets, cm

k_f thermal conductivity coefficient for the fuel watt/cm °C

k_c thermal conductivity coefficient for the clad watt/cm °C

q_A reference value of the power density, watt/cm^3

q_B estimated value of the power density, watt/cm^3

For the calculations, the variables given above were assigned the following values:

$q_A = 750$ watt/cm^3

$k_f = 0.031$ watt/cm °C

$k_c = 0.138$ watt/cm °C

$q_B = q_A[\frac{e}{100}+1]$